

Calculated Refractivity of Water Vapor and Moist Air in the Atmospheric Window at 10 μm

Richard J. Mathar

Goethestr. 22, 69151 Neckargemünd, Germany

The HITRAN2000 database of infrared line transitions has been used to calculate the dispersion coefficient of water vapor at room temperature in the atmospheric window up to 25 μm , confirming the equivalent earlier compilation by Hill and Lawrence [Infrared Phys. **26**, 371 (1986)]. We complement this line set by the ultraviolet pseudospectrum of Margoliash and Meath [J. Chem. Phys. **68**, 1426 (1978)] to improve coverage of the near infrared. The effect of admixtures of abundant nitrogen, oxygen, carbon dioxide etc. is predicted on the same calculational basis to synthesize the air representative of the mountain that hosts the Very Large Telescope Interferometer, and found to be small compared with the dominant role of water at wavelengths above 3 μm . © 2003 Optical Society of America

OCIS codes: 010.7340,260.2030,260.3060,010.1290

1. Scope

The refractive index of humid air in the middle infrared is of interest to ground-based Astronomy that exploits the atmospheric windows of the electromagnetic spectrum. Atmospheric refraction introduces pointing mismatches,¹ needs correction if sensors of the zero optical path difference are combined with interferometric instruments that work at other

wavelengths and are located tens of meters apart^{2,3} as baselines become large, and effects Adaptive Optics⁴ and models of turbulence.⁵⁻⁷

Yet the applicable experimental results in the windows around 3.5, 4.8 and 10 micron reduce to merely two measurements^{8,9} at wavelengths of $\lambda = 3.4$ and $10.6 \mu\text{m}$, and one¹⁰ at $28 \mu\text{m}$ that does not allow to separate water and dry air easily. The majority of associated data in the literature extends wavelength coverage by extrapolation of mid-infrared or visible¹¹⁻¹³ spectra. Another tempting extrapolation of liquid water data¹⁴⁻¹⁸ via Clausius-Mossotti-(Lorentz-Lorenz)-type density scaling is challenged to account for the strong permanent dipole moment of the water molecules.¹⁹

We present the calculated refractive index n of moist air for λ up to $20 \mu\text{m}$ by accumulating oscillator strengths that stretch over the electromagnetic spectrum from the far ultraviolet to the far infrared.

2. HITRAN Calculation

The cross sections and wavenumbers of the HITRAN database²⁰⁻²⁴ of infrared transitions, augmented by oscillator strengths in the ultraviolet spectrum, serve to calculate the dielectric function of gas mixtures, repeating earlier calculations,^{25,26} but staying away from Golovko's²⁶ modified Clausius-Mossotti scaling. The calculated complex-valued dielectric function ϵ is the response of a superposition of independent oscillators

$$\epsilon(\omega) = 1 + \frac{e^2}{m\epsilon_0} \sum_m N_m \sum_l \frac{f_{ml}}{2\omega_{0ml}} \left[\frac{1}{\omega + \omega_{0ml} - \frac{i}{2}\Gamma_{ml}} - \frac{1}{\omega - \omega_{0ml} - \frac{i}{2}\Gamma_{ml}} \right] \quad (1)$$

with molecule number densities N_m , oscillator strengths f_{ml} , transition frequencies $\omega_{0ml}/(2\pi)$ and full line widths at half maximum Γ_{ml} . e is the elementary charge unit, m the electron

rest mass, and ϵ_0 the permittivity of the vacuum (SI units). The oscillator strengths are derived from the squared transition matrix elements R^2 of the database as

$$f_{ml} = \frac{2mc\omega_{0ml}}{3\hbar e^2} R^2, \quad (2)$$

where \hbar is the reduced Planck constant, c the velocity of light. The complex-valued refractive index is calculated as $n = \sqrt{\epsilon}$ at the wavelengths $\lambda = 2\pi c/\omega$ of interest. The natural density parameters with Eq. (1) are the number densities N_m . To be economical, these will label the subsequent results, as one single number density represents an entire line in a pressure-temperature plot. At places further down where literature data or formulas come into play that do not necessarily adhere to models of independent linear superposition of the molecular dielectric responses, these number densities must be detailed as *specific* pairs of (partial) pressures and temperatures. Scientific standards demand that we also quote those pressures and temperatures to allow reproduction of all results.

The bare output of taking two molecule species of the HITRAN database that dominate the near-IR dispersion is shown in Fig. 1: water configured by summing l in Eq. (1) over 31,646 lines that populate the wavelength interval between 441 nm and 24.96 mm, and carbon dioxide configured by 27,123 lines that populate the interval between 1.036 μm and 22.6 μm . The figure illustrates the importance of the anomalous dispersion due to carbon dioxide^{27,28} in the region 3.5–5 μm (L and M band).

The density parameters are equivalent to the partial pressures at the site of the Very Large Telescope Interferometer²⁹ and could be scaled to other atmospheres by use of the ideal gas equation.

3. Pure Water Vapor

The drawback of the previous model calculation is the neglect of the absorption spectrum at high excitation energies and of the photoionization continuum, which induces two artifacts in the calculated index of refraction: (i) removal of an almost constant, featureless “background” in the mid- and far-infrared. (ii) omission of the rise towards short wavelengths, which is replaced by a flat extrapolation through to $n \xrightarrow{\lambda \rightarrow 0} 1$. The remedy chosen in Fig. 2 is to add the ten pseudo-oscillators of Table I by Margoliash and Meath,³⁰ all at nominal wavelengths below 178.1 nm. The figure shows

- that these lift n by about 9×10^{-7} —an amount that is proportional to the molecular density—, which now matches the laboratory gas cell data measured by Matsumoto,^{8,9}
- that strong dispersion is added if λ is shorter than about $1.5 \mu\text{m}$.

The dashed line is the fitting Eq. (14) of Hill and Lawrence²⁵ for the same density of 2.9907 g/m^3 and a temperature of $12 \text{ }^\circ\text{C}$, which might be too simplistic between 2 and $6 \mu\text{m}$ for some applications. In comparison to their procedure²⁵ (i) this here does not retro-fit experimental data of the visible spectrum to add a single pseudo-oscillator representative of this part of the spectrum—but employs ten pseudo-oscillators that represent dipole oscillator strength distributions which are reproducible by ab-initio calculations,³¹ (ii) this here does not employ an empirical scaling factor of 1.045.

Results obtained with the 31,683 water lines of the 2001 HITRAN edition³² differ indiscernibly from those of the 2000 edition for all figures displayed here.

Note in the margin: If the calculation of Fig. 2 were continued to $311 \mu\text{m}$ and $337 \mu\text{m}$, refractivities of $+2.61 \times 10^{-5}$ and $+2.12 \times 10^{-5}$, respectively, would result. This deviates by only 4 % and 6 %, respectively, from the associated experimental data by Bradley and Gebbie¹⁰ (in their Fig. 2) after scaling to a density of $4.844 \times 10^{23} \text{ m}^{-3}$, i.e., their pressure and temperature.

The next section reveals why just digitizing the Hill–Clifford–Lawrence lineshape graphs³³ is not an option to start our subsequent analysis of air, and an independent implementation is inevitable: (i) the graphs had been limited to $\lambda > 5.7 \mu\text{m}$, and (ii) they exclusively dealt with pure water vapor.

4. Moist Air

A. *Representative Atoms and Molecules*

Fig. 3 and Fig. 4 synthesize a moist air model at the vapor density as in Fig. 2 and at a nominal air pressure of 752.9 hPa (sum of the partial pressures of the dry components). “Nominal” means, 752.9 hPa was assumed to derive molecular densities based on world averages of volume percentages; the sum of all partial pressures of the eight molecule species that actually build our dry air model is 746.64 hPa. The HITRAN line list is the basis and bolstered further by the following, much less resolved line sets:

- For N_2 , O_2 , H_2O and CH_4 : Ten pseudo-spectral lines each as listed by Margoliash and Meath.³⁰
- For CO_2 : The discrete and continuum transitions by Padiyal et al.³⁴ (their tables III–VIII and Fig. 8).

- For Ar: two transitions at $\hbar\omega_{0ml} = 11.62$ and 11.83 eV in Eggarter's³⁵ Table III, plus twelve transitions between 13.864 and 15.188 eV taken from Table V by Chan et al.,^{36,37} plus 450 “histogram” transitions between 16.0 and 500 eV taken from Table I by Chan et al.³⁶ These add up to an oscillator strength sum of $S(0) \approx 13.3$ which indicates that the four core electrons bound by 119 and 12 Hartree^{35,38} are not yet accounted for at 500 eV.
- For Ne: five transitions between 743.7 Å and 618.7 Å from Table VIII by Hibbert et al.,³⁹ plus 250 transitions between 21.6 eV and 250 eV taken from Table V by Chan et al.⁴⁰

Fig. 3 in comparison with the upper left corner of Fig. 2 shows that the dispersion at wavelengths below 2.5 μm is governed by the dry air components, not by water. Crosses in the figure represent the Ciddor fit⁴¹ to wet air; the inputs are 12 °C, 746.64 hPa dry air with 370 ppm CO_2 , and 3.94 hPa water.

At $\lambda = 10$ μm , the calculated background refractivity of the *dry* components is about 1.6×10^{-6} smaller than the Ciddor formula⁴¹ for 752.9 hPa, but only about 1.5×10^{-7} smaller than the Ciddor formula for 746.64 hPa. (A graphics of these featureless dry air data is omitted here. A preview on the similar flat horizontal in Fig. 5 illustrates that it would not add information.) Recalling that the response of the oscillators in Eq. (1) is linear at all wavelengths, this comparison in the flat side lobes far away from all resonances demonstrates rather complete sampling of the air constituents, and gives confidence that the rise of n at short wavelengths in Fig. 3 is quantitatively correct. [The Ciddor formula summons experimental data up to 1.7 μm . Stretching it here much beyond this wavelength

indicates that we are not aware of any better suitable compilation to compare with; it does not mean we claim validity beyond the original author's intent.]

B. Negligible Gas Components

The estimated contribution of the following gases to the refractive index of standard air remains tiny in the wavelength region shown: (i) At most $n < 1.3 \times 10^{-10}$ would be added by introducing $2.69 \times 10^{25} \text{ m}^{-3}$ He—estimated by density scaling of the Migneron and Levinger value⁴² at $\lambda = 700 \text{ nm}$. (ii) About $n \approx 1.05 \times 10^{-10}$ could be added through $5.7 \times 10^{18} \text{ m}^{-3}$ N_2O , estimated on the basis of ten pseudo-oscillators.³⁰ (iii) The contribution of $1.9 \times 10^{19} \text{ m}^{-3}$ Kr is $n \approx 3 \times 10^{-10}$ derived from the Chan et al.³⁶ spectra. (iv) The HITRAN transitions predict a change of up to -2×10^{-11} for $7.6 \times 10^{18} \text{ m}^{-3}$ NH_3 , which becomes about $+1 \times 10^{-10}$ if we add ten pseudo-oscillators.³⁰

C. Bradley-Gebbie 28 micron datum

In Fig. 5, we calculate this synthetic air model with molecular densities that build up 833.3 hPa at 26 °C, and compare with an interferometric measurement at a 28 μm water maser line.¹⁰ (The Ciddor⁴¹ index of refraction is $n - 1 = 2.159 \times 10^{-4}$ at 833.3 hPa of dry air at this temperature and wavelength.) We do not have a plausible explanation of why the calculated $n - 1$ is about 0.25×10^{-4} lower than the experimental value of $(2.3 \pm 0.1) \times 10^{-4}$: Fig. 5 demonstrates that even a 100 % error in the assumed water content could at most lift the calculated values to the flat line of dry air, which still remains 6 % below the experiment. If we even start from *liquid* water measured⁴³ at $n - 1 = 0.363$, a linear scaling of the density of the liquid, $3.344 \times 10^{28} \text{ m}^{-3}$ to the density of the gas, $2.97 \times 10^{23} \text{ m}^{-3}$,

leaves $n - 1 \approx 3 \times 10^{-6}$ —more accurate Clausius-Mossotti scaling twice as much—, which still is too small to bridge the gap between the dry air calculation and the measured point in Fig. 5. However, the refractivity of pure N₂ provided by Bradley and Gebbie, 2.26×10^{-4} in their¹⁰ Fig. 1, fits rather well with our calculated 2.31×10^{-4} of pure N₂ at 833.3 hPa.

5. Summary

A full calculation of water vapor dispersion founded on the HITRAN line set suffers a priori from incomplete assessment of atomic and molecular line transitions—including transitions into the continuum—at visible and UV wavelengths, which limits its validity to about $\lambda > 2.5 \mu\text{m}$. Employing other sets of (coarse grained) dipole oscillator strength distributions found in the literature extends the validity into the near infrared. In conclusion, the first fit-free calculation of the refractivity of moist air at all non-precipitable water vapor concentrations in the entire Infrared at variable temperature, pressure and composition has been demonstrated. Fitting parameters to adjust the calculation to a background dielectric constant are absent, nor are assumptions made or necessary of how the results grown out of infrared line data interpolate to spectra in the visible.

Verification of those calculated mid-Infrared refractivities is most of all limited by the unexpectedly sketchy coverage by hands-on experiments. A prime cause to this is the widely destructive (costly) influence of water on lense and beamsplitter materials of infrared optics.⁴⁴

A discrepancy to a published experimental value¹⁰ at $28 \mu\text{m}$ remains.

References

1. T. A. Livengood, K. E. Fast, T. Kostiuk, F. Espenak, D. Buhl, J. J. Goldstein, T. Hewagama, and K. H. Ro, “Refraction by Earth’s Atmosphere near 12 Microns,” *Publ. Astr. Soc. Pacific* **111**, 512–521 (1999).
2. J. A. Meisner and R. S. Le Poole, “Dispersion affecting the VLTI and 10 micron interferometry using MIDI,” in *Interferometry for Optical Astronomy II*, W. A. Traub, ed., *Proc. SPIE* **4838**, 609–624 (2003).
3. H. Hogenhuis, M. Visser, G. Ruwiel, F. Hommes, A. Wielders, and A. Couwenberg, “Test results of the VLTI Delay line verification program,” in *Interferometry in Optical Astronomy*, P. J. Lena and A. Quirrenbach, eds., *Proc. SPIE* **4006**, 198–206 (2000).
4. J. Vaillant, E. Thiébaud, and M. Tallon, “ELPOA: Data processing of chromatic differences of the tilt measured with a polychromatic laser guide star,” in *Adaptive Optical Systems Technology*, P. L. Wizinowich, ed., *Proc. SPIE* **4007**, 308–315 (2000).
5. O. P. Lay, “The temporal power spectrum of atmospheric fluctuations due to water vapor,” *Astron. Astrophys. Suppl. Ser.* **122**, 535–545 (1997).
6. O. P. Lay, “Phase calibration and water vapor radiometry for millimeter-wave arrays,” *Astron. Astrophys. Suppl. Ser.* **122**, 547–557 (1997).
7. R. L. Akeson, M. R. Swain, and M. M. Colavita, “Differential phase technique with the Keck Interferometer,” in *Interferometry in Optical Astronomy*, P. J. Lena and A. Quirrenbach, eds., *Proc. SPIE* **4006**, 321–327 (2000).
8. H. Matsumoto, “The refractive index of moist air in the 3- μ m region,” *Metrologia* **18**, 49–52 (1982).

9. H. Matsumoto, "The refractivities of water vapour for CO₂ laser lines," *Opt. Comm.* **50**, 356–358 (1984).
10. C. C. Bradley and H. A. Gebbie, "Refractive Index of Nitrogen, Water Vapor, and their Mixtures at submillimeter Wavelengths," *Appl. Opt.* **10**, 755–758 (1971).
11. J. Beers and T. Doiron, "Verification of revised Water Vapour Correction to the Refractive Index of Air," *Metrologia* **29**, 315–316 (1992).
12. K. P. Birch and M. J. Downs, "Correction to the updated Edlén equation for the Refractive Index of Air," *Metrologia* **31**, 315–316 (1994).
13. K. P. Birch and M. J. Downs, "The result of a comparison between calculated and measured values of the refractive index of air," *J. Phys. E* **21**, 694–695 (1988).
14. M. Centeno V., "The Refractive Index of Liquid Water in the Near Infra-Red Spectrum," *J. Opt. Soc. Am.* **31**, 244–247 (1941).
15. R. Penndorf, "Tables of the refractive index of standard air and the Rayleigh scattering coefficient for the spectral region between 0.2 and 20.0 μ and their application to atmospheric optics," *J. Opt. Soc. Am.* **47**, 176–182 (1957).
16. P. S. Ray, "Broadband Complex Refractive Indices of Ice and Water," *Appl. Opt.* **11**, 1836–1844 (1972).
17. P. D. T. Huibers, "Models of the wavelength dependence of the index of refraction of water," *Appl. Opt.* **36**, 3785–3787 (1997).
18. A. B. Djurišić and B. V. Stanić, "Modeling the Wavelength Dependence of the Index of Refraction of Water in the range of 200 nm to 200 μ m," *Appl. Opt.* **37**, 2696–2698 (1998).

19. D. G. Archer and P. Wang, "The dielectric constant of Water and Debye-Hückel Limiting Law Slopes," *J. Phys. Chem. Ref. Data* **19**, 371–411 (1990).
20. L. S. Rothman, C. P. Rinsland, A. Goldman, S. T. Massie, D. P. Edwards, J.-M. Flaud, A. Perrin, C. Camy-Peyret, V. Dana, J.-Y. Mandin, J. Schroeder, A. Mccann, R. R. Gamache, R. B. Wattson, K. Yoshino, K. V. Chance, K. W. Jucks, L. R. Brown, V. Nemtchinov, and P. Varanasi, "The HITRAN Molecular Spectroscopic Database and HAWKS (HITRAN Atmospheric workstation): 1996 Edition," *J. Quant. Spectr. & Radiat. Transfer* **60**, 665–710 (1998).
21. R. A. Toth, "Analysis of Line Positions and Strengths of H_2^{16}O Ground and Hot Bands Connecting to Interacting Upper States: (020), (100), and (001)," *J. Mol. Spectr.* **194**, 28–42 (1999).
22. A. Goldman, R. R. Gamache, A. Perrin, J.-M. Flaud, C. P. Rinsland, and L. S. Rothman, "HITRAN partition functions and weighted transition-moments squared," *J. Quant. Spectr. & Radiat. Transfer* **66**, 455–486 (2000).
23. L. P. Giver, C. Chackerian Jr., and P. Varanasi, "Visible and near-infrared H_2^{16}O line intensity corrections for HITRAN-96," *J. Quant. Spectr. & Radiat. Transfer* **66**, 101–105 (2000).
24. U. G. Jørgensen, P. Jensen, G. O. Sørensen, and B. Aringer, " H_2O in stellar atmospheres," *Astron. Astrophys.* **372**, 249–259 (2001).
25. R. J. Hill and R. S. Lawrence, "Refractive Index of water Vapor in Infrared Windows," *Infrared Phys.* **26**, 371–376 (1986).
26. V. F. Golovko, "Dispersion formula and continuous absorption of water vapor," *J.*

- Quant. Spectr. & Radiat. Transfer **65**, 621–644 (2000).
27. P. E. Ciddor, “Refractive Index of Air, 3. the roles of CO₂, H₂O and refractivity virials,” Appl. Opt. **41**, 2292–2298 (2002).
 28. P. E. Ciddor, “Erratum: Refractive Index of Air, 3. the roles of CO₂, H₂O and refractivity virials,” Appl. Opt. **41**, 7036–7036 (2002).
 29. M. Sarazin, “Astroclimatology of Paranal,” Tech. rep., European Southern Observatory (1999). <http://www.eso.org/gen-fac/pubs/astclim/paranal>
 30. D. J. Margoliash and W. J. Meath, “Pseudospectral dipole oscillator strength distributions and some related two body interaction coefficients for H, He, Li, N, O, H₂, N₂, O₂, NO, N₂O, H₂O, NH₃ and CH₄,” J. Chem. Phys. **68**, 1426–1431 (1978).
 31. D. Spelsberg and W. Meyer, “Ab initio dynamic multipole polarizabilities and hyperpolarizabilities of H₂O and the long-range interaction coefficients for its dimer,” J. Chem. Phys. **108**, 1532–1543 (1998).
 32. L. S. Rothman, A. Barbe, D. C. Benner, L. R. Brown, C. Camy-Peyret, M. R. Carleer, K. Chance, C. Clerbaux, V. Dana, V. M. Devi, A. Fayt, J.-M. Flaud, R. R. Gamache, A. Goldman, D. Jacquemart, K. W. Jucks, W. J. Lafferty, J.-Y. Mandin, S. T. Massie, V. Nemtchinov, D. A. Newnham, A. Perrin, C. P. Rinsland, J. Schroeder, K. M. Smith, M. A. H. Smith, K. Tang, R. A. Toth, J. V. Auwera, P. Varanasi, and K. Yoshino, “The HITRAN molecular spectroscopic database: edition of 2000 including updates through 2001,” J. Quant. Spectr. & Radiat. Transfer **82**, 5–44 (2003).
 33. R. J. Hill, S. F. Clifford, and R. S. Lawrence, “Refractive-index and absorption fluctuations in the infrared caused by temperature, humidity, and pressure fluctuations,” J.

- Opt. Soc. Am. **70**, 1192–1205 (1980).
34. N. Padial, G. Csanak, B. V. McKoy, and P. W. Langhoff, “Photoexcitation and ionization in carbon dioxide: Theoretical studies in the separated-channel static-exchange approximation,” Phys. Rev. A **23**, 218–235 (1981).
 35. E. Eggarter, “Comprehensive optical and collision data for radiation action. II. Ar,” J. Chem. Phys. **62**, 833–847 (1975).
 36. W. F. Chan, G. Cooper, X. Guo, G. R. Burton, and C. E. Brion, “Absolute optical oscillator strengths for the electronic excitation of atoms at high resolution. III. The photoabsorption of argon, krypton, and xenon,” Phys. Rev. A **46**, 149–171 (1992).
 37. W. F. Chan, G. Cooper, X. Guo, G. R. Burton, and C. E. Brion, “Erratum: Absolute optical oscillator strengths for the electronic excitation of atoms at high resolution. III. The photoabsorption of argon, krypton, and xenon,” Phys. Rev. A **48**, 858–860 (1993).
 38. C. F. Bunge, J. A. Barrientos, and A. V. Bunge, “Roothaan-Hartree-Fock Ground-State Atomic Wave Functions: Slater-Type Orbital Expansions and Expectation Values for $Z = 2-54$,” Atom. Data Nucl. Data Tab. **53**, 113–162 (1993).
 39. A. Hibbert, M. Le Dourneuf, and M. Mohan, “Energies, oscillator strengths, and lifetimes for neon-like ions up to Kr XXVII,” Atom. Data Nucl. Data Tab. **53**, 23–112 (1993).
 40. W. F. Chan, G. Cooper, X. Guo, and C. E. Brion, “Absolute optical oscillator strengths for the electronic excitation of atoms at high resolution. II. The photoabsorption of neon,” Phys. Rev. A **45**, 1420–1433 (1992).
 41. P. E. Ciddor, “Refractive Index of Air: New Equations for the Visible and Near In-

frared,” Appl. Opt. **35**, 1566–1573 (1996).

42. R. Migneron and J. S. Levinger, “Index of Refraction and Sum Rules for Helium,” Phys. Rev. **139**, 646–648 (1965).

43. G. M. Hale and M. R. Querry, “Optical Constants of Water in the 200 nm to 200 μm Wavelength Region,” Appl. Opt. **12**, 555–563 (1973).

44. F. Hase (2003), priv. commun.

List of Figure captions

Fig. 1. Solid curve: Dispersion of a gas mixture of water (density of 10^{23} molecules/m³) and CO₂ (density of 7.076×10^{21} molecules/m³) calculated from the HITRAN data base alone. Dashed curve: the dispersion of the pure water vapor (10^{23} molecules/m³).

Fig. 2. Solid line: Calculated water vapor dispersion at $N_m = 10^{23}$ molecules/m³. The isolated squares near 3.4 and 10.6 μm are Matsumoto's data^{8,9} scaled to the same molecular density; the dashed line is the Hill-Lawrence fit.

Fig. 3. This solid line repeats the calculation of Fig. 2 and adds more gas species: N₂ at a density of 1.49×10^{25} m⁻³, O₂ at 3.84×10^{24} m⁻³, Ar at 1.786×10^{23} m⁻³, CO₂ at 7.076×10^{21} m⁻³, Ne at 3.44×10^{20} m⁻³, CH₄ at 3.06×10^{19} m⁻³, O₃ at 2.23×10^{18} m⁻³, and CO at 1.91×10^{18} m⁻³. Crosses are wet air according to Ciddor's⁴¹ App. B.

Fig. 4. Continuation of Fig. 3 into the range $6 \mu\text{m} \leq \lambda \leq 22 \mu\text{m}$. CO₂ bands near 15 μm separate two windows of high transmission through the earth's atmosphere that astronomers call the N band (7.5–14.5 μm) and the Q band (17–25 μm).

Fig. 5. Isolated square: Table I of Bradley-Gebbie.¹⁰ Solid ragged line: calculated humid air at a total pressure of 833.3 hPa (821.0 hPa dry air components plus 12.3 hPa or 2.97×10^{23} m⁻³ water). Dashed ragged line: calculated 821.4 hPa dry air plus 11.9 hPa water—that is a 3.3 % change in water content relative to the solid ragged line, chosen to visualize the 3.3 % error estimate in Table I.¹⁰ Flat horizontal: calculated 833.3 hPa dry air.

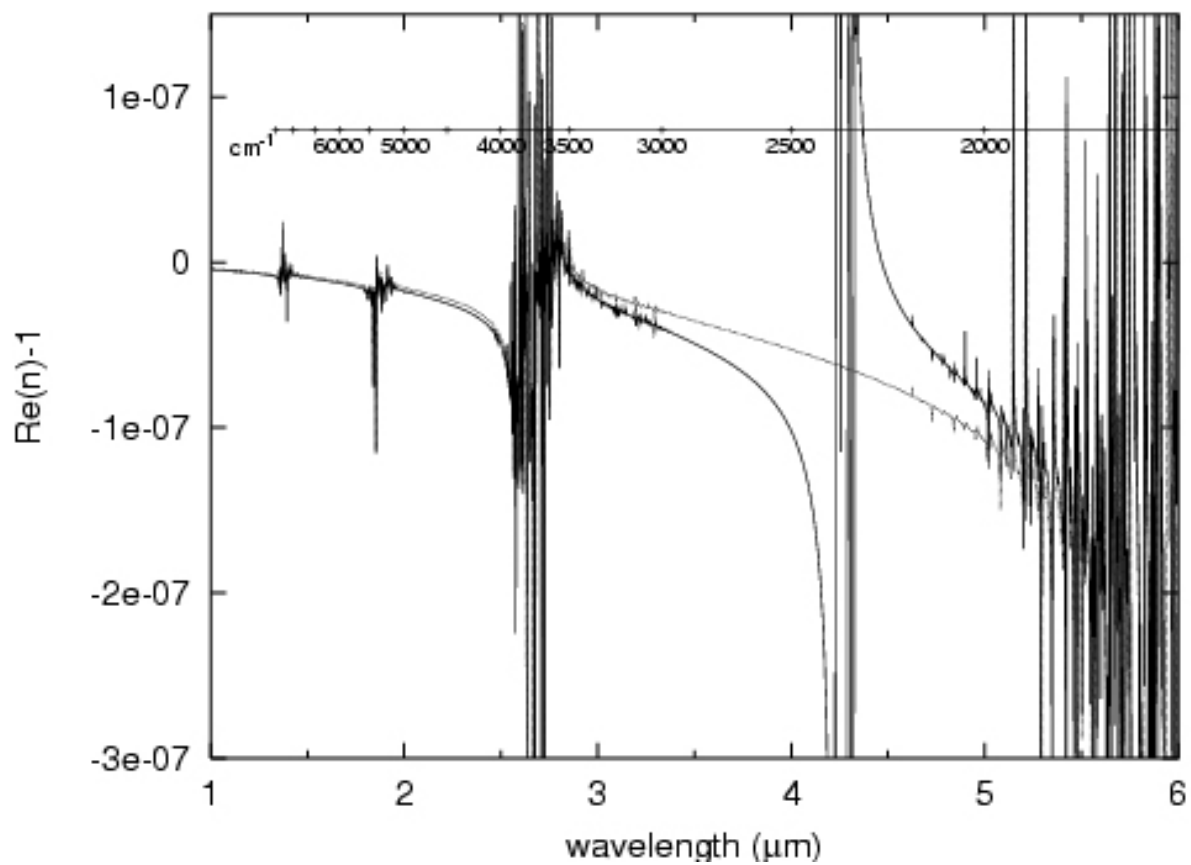


Fig. 1. Solid curve: Dispersion of a gas mixture of water (density of 10^{23} molecules/m³) and CO₂ (density of 7.076×10^{21} molecules/m³) calculated from the HITRAN data base alone. Dashed curve: the dispersion of the pure water vapor (10^{23} molecules/m³). matharF1.ps

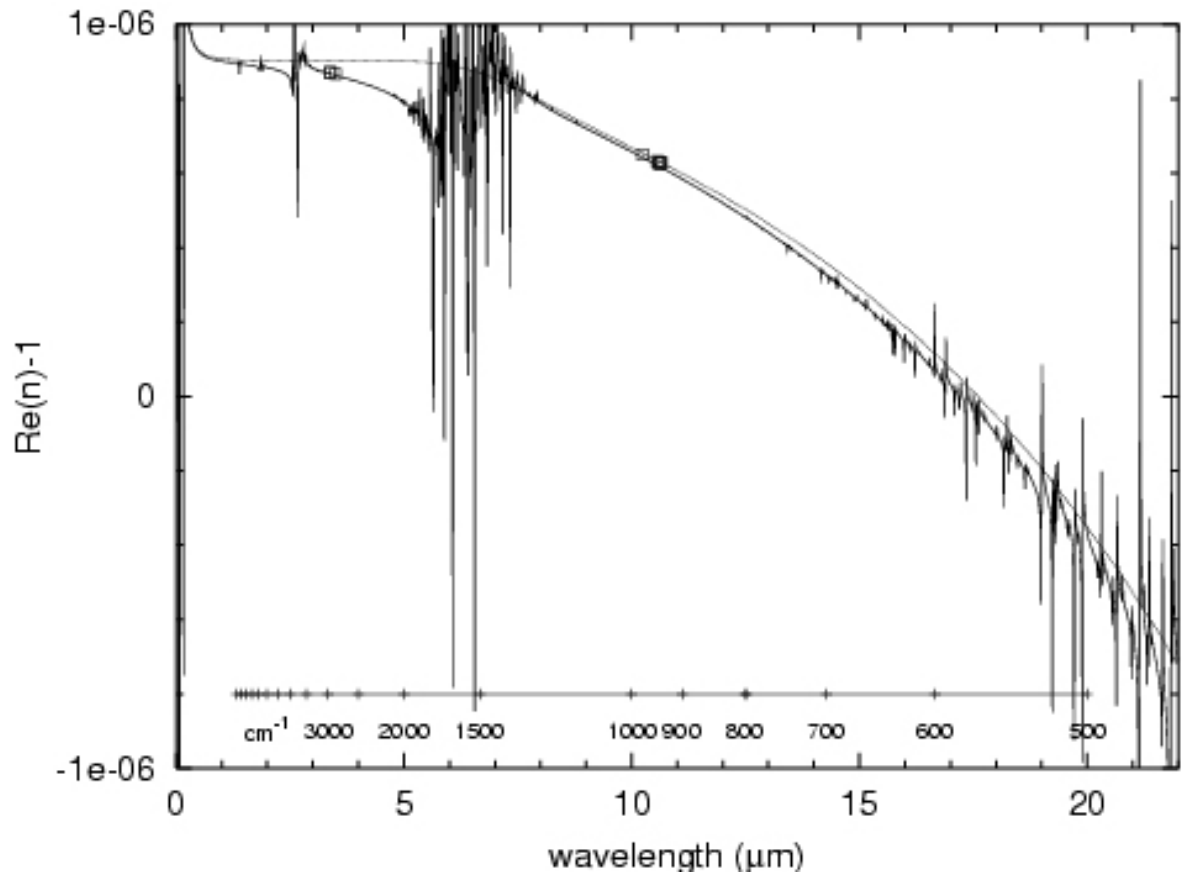


Fig. 2. Solid line: Calculated water vapor dispersion at $N_m = 10^{23}$ molecules/m³. The isolated squares near 3.4 and 10.6 μm are Matsumoto's data^{8,9} scaled to the same molecular density; the dashed line is the Hill-Lawrence fit. matharF2.ps

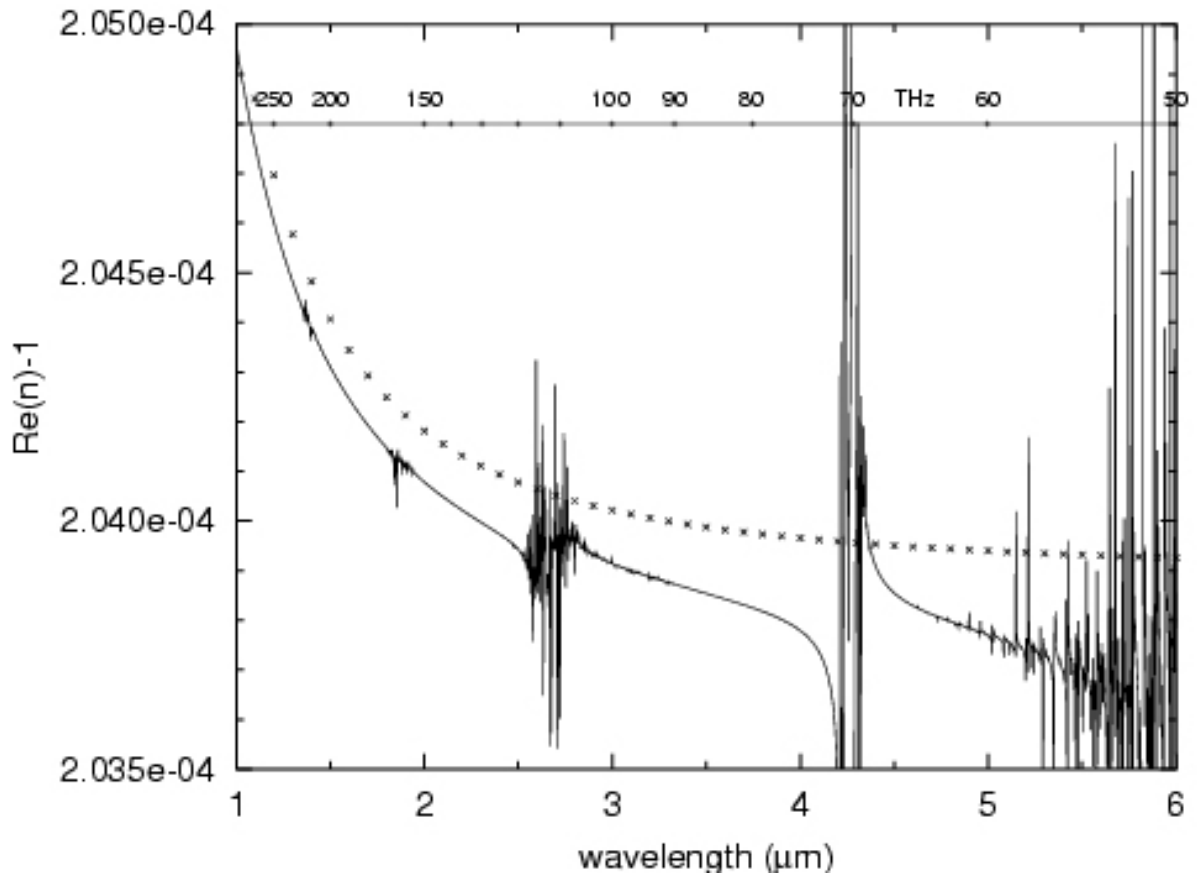


Fig. 3. This solid line repeats the calculation of Fig. 2 and adds more gas species: N_2 at a density of $1.49 \times 10^{25} \text{ m}^{-3}$, O_2 at $3.84 \times 10^{24} \text{ m}^{-3}$, Ar at $1.786 \times 10^{23} \text{ m}^{-3}$, CO_2 at $7.076 \times 10^{21} \text{ m}^{-3}$, Ne at $3.44 \times 10^{20} \text{ m}^{-3}$, CH_4 at $3.06 \times 10^{19} \text{ m}^{-3}$, O_3 at $2.23 \times 10^{18} \text{ m}^{-3}$, and CO at $1.91 \times 10^{18} \text{ m}^{-3}$. Crosses are wet air according to Ciddor's⁴¹ App. B. matharF3.ps

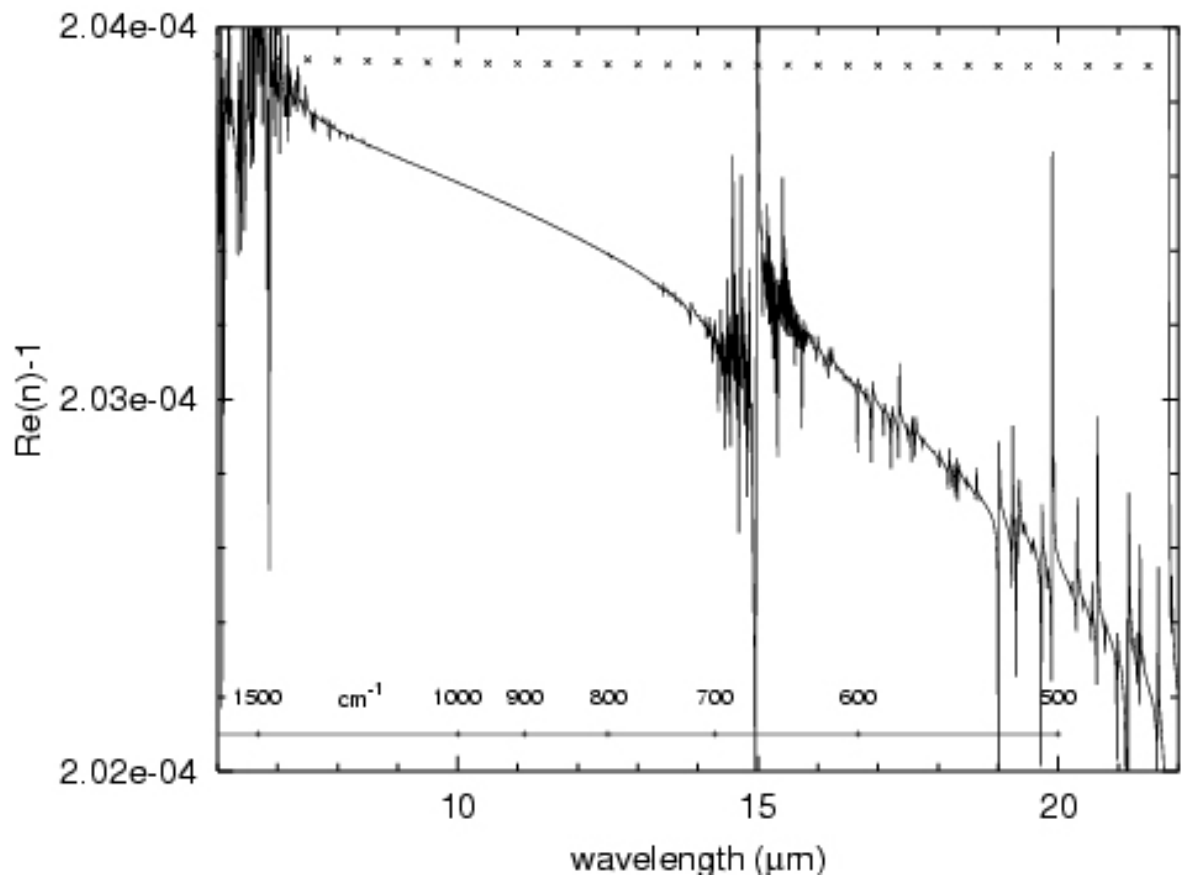


Fig. 4. Continuation of Fig. 3 into the range $6 \mu\text{m} \leq \lambda \leq 22 \mu\text{m}$. CO_2 bands near $15 \mu\text{m}$ separate two windows of high transmission through the earth's atmosphere that astronomers call the N band ($7.5\text{--}14.5 \mu\text{m}$) and the Q band ($17\text{--}25 \mu\text{m}$). math-arF4.ps

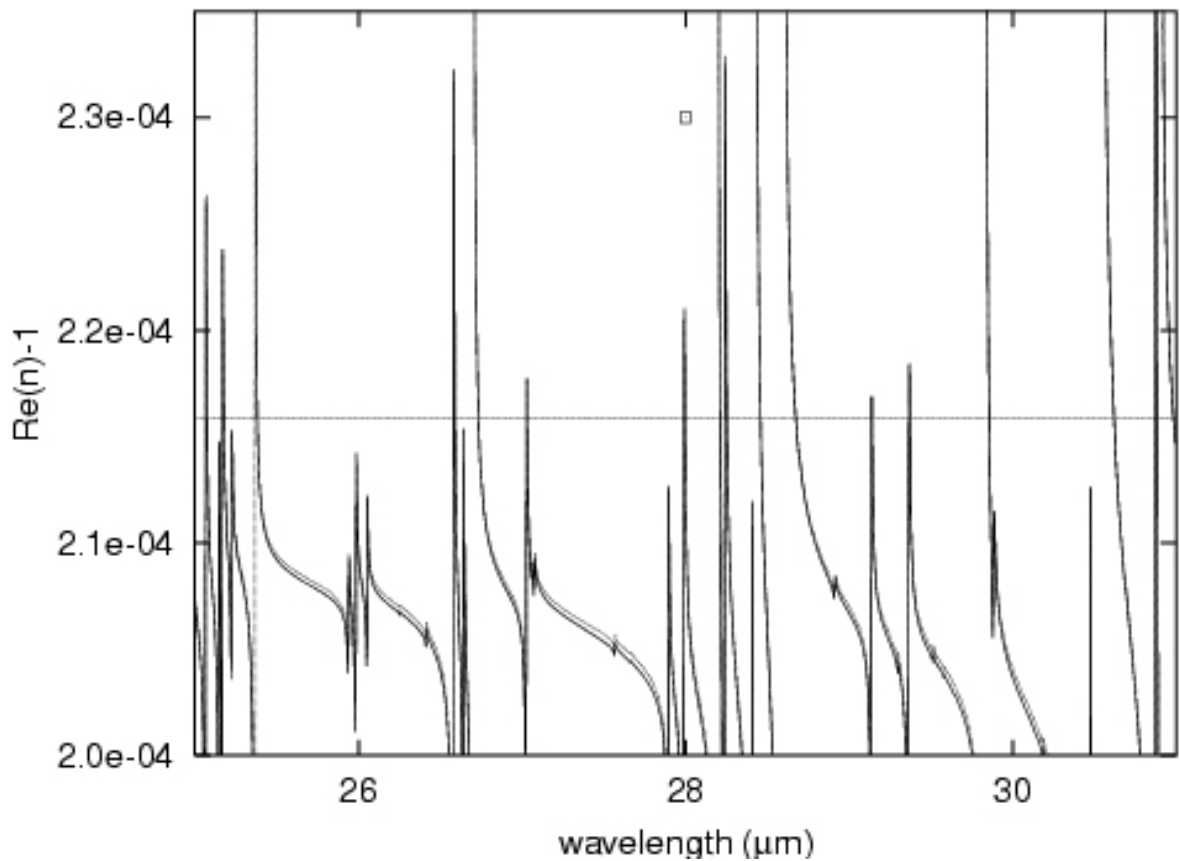


Fig. 5. Isolated square: Table I of Bradley-Gebbie.¹⁰ Solid ragged line: calculated humid air at a total pressure of 833.3 hPa (821.0 hPa dry air components plus 12.3 hPa or $2.97 \times 10^{23} \text{ m}^{-3}$ water). Dashed ragged line: calculated 821.4 hPa dry air plus 11.9 hPa water—that is a 3.3 % change in water content relative to the solid ragged line, chosen to visualize the 3.3 % error estimate in Table I.¹⁰ Flat horizontal: calculated 833.3 hPa dry air. matharF5.ps